

A measurement of the t dependence of the helicity structure of diffractive ρ meson electroproduction at HERA

H1 Collaboration

Abstract

The helicity structure of the diffractive electroproduction of ρ mesons, $e+p \rightarrow e+\rho+Y$, is studied in a previously unexplored region of large four-momentum transfer squared at the proton vertex, t : $0 < t' < 3 \text{ GeV}^2$, where $t' = |t| - |t|_{min}$. The data used are collected with the H1 detector at HERA in the kinematic domain $2.5 < Q^2 < 60 \text{ GeV}^2$, $40 < W < 120 \text{ GeV}$. No t dependence of the r_{00}^{04} spin density matrix element is found. A significant t dependent helicity non-conservation from the virtual photon to the ρ meson is observed for the spin density matrix element combinations $r_{00}^5 + 2r_{11}^5$ and $r_{00}^1 + 2r_{11}^1$. These t dependences are consistently described by a perturbative QCD model based on the exchange of two gluons.

C. Adloff³³, V. Andreev²⁴, B. Andrieu²⁷, T. Anthonis⁴, V. Arkadov³⁵, A. Astvatsatourov³⁵,
 A. Babaev²³, J. Bähr³⁵, P. Baranov²⁴, E. Barrelet²⁸, W. Bartel¹⁰, J. Becker³⁷, A. Beglarian³⁴,
 O. Behnke¹³, C. Beier¹⁴, A. Belousov²⁴, Ch. Berger¹, T. Berndt¹⁴, J.C. Bizot²⁶, J. Böhme¹⁰,
 V. Boudry²⁷, W. Braunschweig¹, V. Brisson²⁶, H.-B. Bröker², D.P. Brown¹⁰, W. Brückner¹²,
 D. Bruncko¹⁶, J. Bürger¹⁰, F.W. Büsser¹¹, A. Bunyatyan^{12,34}, A. Burrage¹⁸, G. Buschhorn²⁵,
 L. Bystritskaya²³, A.J. Campbell¹⁰, J. Cao²⁶, S. Caron¹, F. Cassol-Brunner²², D. Clarke⁵,
 B. Clerbaux⁴, C. Collard⁴, J.G. Contreras^{7,41}, Y.R. Coppens³, J.A. Coughlan⁵,
 M.-C. Cousinou²², B.E. Cox²¹, G. Cozzika⁹, J. Cvach²⁹, J.B. Dainton¹⁸, W.D. Dau¹⁵,
 K. Daum^{33,39}, M. Davidsson²⁰, B. Delcourt²⁶, N. Delerue²², R. Demirchyan³⁴,
 A. De Roeck^{10,43}, E.A. De Wolf⁴, C. Diaconu²², J. Dingfelder¹³, P. Dixon¹⁹, V. Dodonov¹²,
 J.D. Dowell³, A. Droutskoi²³, A. Dubak²⁵, C. Duprel², G. Eckerlin¹⁰, D. Eckstein³⁵,
 V. Efremenko²³, S. Egli³², R. Eichler³⁶, F. Eisele¹³, E. Eisenhandler¹⁹, M. Ellerbrock¹³,
 E. Elsen¹⁰, M. Erdmann^{10,40,e}, W. Erdmann³⁶, P.J.W. Faulkner³, L. Favart⁴, A. Fedotov²³,
 R. Felst¹⁰, J. Ferencei¹⁰, S. Ferron²⁷, M. Fleischer¹⁰, Y.H. Fleming³, G. Flügge²,
 A. Fomenko²⁴, I. Foresti³⁷, J. Formánek³⁰, G. Franke¹⁰, E. Gabathuler¹⁸, K. Gabathuler³²,
 J. Garvey³, J. Gassner³², J. Gayler¹⁰, R. Gerhards¹⁰, C. Gerlich¹³, S. Ghazaryan^{4,34},
 L. Goerlich⁶, N. Gogitidze²⁴, C. Grab³⁶, V. Grabski³⁴, H. Grässler², T. Greenshaw¹⁸,
 G. Grindhammer²⁵, T. Hadig¹³, D. Haidt¹⁰, L. Hajduk⁶, J. Haller¹³, W.J. Haynes⁵,
 B. Heinemann¹⁸, G. Heinzelmann¹¹, R.C.W. Henderson¹⁷, S. Hengstmann³⁷, H. Henschel³⁵,
 R. Heremans⁴, G. Herrera^{7,44}, I. Herynek²⁹, M. Hildebrandt³⁷, M. Hilgers³⁶, K.H. Hiller³⁵,
 J. Hladký²⁹, P. Höting², D. Hoffmann²², R. Horisberger³², A. Hovhannisyan³⁴, S. Hurling¹⁰,
 M. Ibbotson²¹, Ç. İssever⁷, M. Jacquet²⁶, M. Jaffre²⁶, L. Janauschek²⁵, X. Janssen⁴,
 V. Jemanov¹¹, L. Jönsson²⁰, C. Johnson³, D.P. Johnson⁴, M.A.S. Jones¹⁸, H. Jung^{20,10},
 D. Kant¹⁹, M. Kapichine⁸, M. Karlsson²⁰, O. Karschnick¹¹, F. Keil¹⁴, N. Keller³⁷,
 J. Kennedy¹⁸, I.R. Kenyon³, S. Kermiche²², C. Kiesling²⁵, P. Kjellberg²⁰, M. Klein³⁵,
 C. Kleinwort¹⁰, T. Kluge¹, G. Knies¹⁰, B. Koblitz²⁵, S.D. Kolya²¹, V. Korbel¹⁰, P. Kostka³⁵,
 S.K. Kotelnikov²⁴, R. Koutouev¹², A. Koutov⁸, H. Krehbiel¹⁰, J. Kroseberg³⁷, K. Krüger¹⁰,
 A. Küpper³³, T. Kuhr¹¹, T. Kurča¹⁶, D. Lamb³, M.P.J. Landon¹⁹, W. Lange³⁵,
 T. Laštovička^{35,30}, P. Laycock¹⁸, E. Lebailly²⁶, A. Lebedev²⁴, B. Leißner¹, R. Lemrani¹⁰,
 V. Lendermann⁷, S. Levonian¹⁰, M. Lindstroem²⁰, B. List³⁶, E. Lobodzinska^{10,6},
 B. Lobodzinski^{6,10}, A. Loginov²³, N. Loktionova²⁴, V. Lubimov²³, S. Lüders³⁶, D. Lüke^{7,10},
 L. Lytkin¹², H. Mahlke-Krüger¹⁰, N. Malden²¹, E. Malinovski²⁴, I. Malinovski²⁴,
 R. Maraček²⁵, P. Marage⁴, J. Marks¹³, R. Marshall²¹, H.-U. Martyn¹, J. Martyniak⁶,
 S.J. Maxfield¹⁸, D. Meer³⁶, A. Mehta¹⁸, K. Meier¹⁴, A.B. Meyer¹¹, H. Meyer³³, J. Meyer¹⁰,
 P.-O. Meyer², S. Mikocki⁶, D. Milstead¹⁸, T. Mkrtchyan³⁴, R. Mohr²⁵, S. Mohrdieck¹¹,
 M.N. Mondragon⁷, F. Moreau²⁷, A. Morozov⁸, J.V. Morris⁵, K. Müller³⁷, P. Murín^{16,42},
 V. Nagovizin²³, B. Naroska¹¹, J. Naumann⁷, Th. Naumann³⁵, G. Nellen²⁵, P.R. Newman³,
 F. Niebergall¹¹, C. Niebuhr¹⁰, O. Nix¹⁴, G. Nowak⁶, J.E. Olsson¹⁰, D. Ozerov²³, V. Panassik⁸,
 C. Pascaud²⁶, G.D. Patel¹⁸, M. Peez²², E. Perez⁹, J.P. Phillips¹⁸, D. Pitzl¹⁰, R. Pöschl²⁶,
 I. Potachnikova¹², B. Povh¹², G. Rädcl¹, J. Rauschenberger¹¹, P. Reimer²⁹, B. Reiser²⁵,
 D. Reyna¹⁰, C. Risler²⁵, E. Rizvi³, P. Robmann³⁷, R. Roosen⁴, A. Rostovtsev²³, S. Rusakov²⁴,
 K. Rybicki⁶, D.P.C. Sankey⁵, S. Schätzel¹³, J. Scheins¹, F.-P. Schilling¹⁰, P. Schleper¹⁰,
 D. Schmidt³³, D. Schmidt¹⁰, S. Schmidt²⁵, S. Schmitt¹⁰, M. Schneider²², L. Schoeffel⁹,
 A. Schöning³⁶, T. Schörner²⁵, V. Schröder¹⁰, H.-C. Schultz-Coulon⁷, C. Schwanenberger¹⁰,
 K. Sedlák²⁹, F. Sefkow³⁷, V. Shekelyan²⁵, I. Sheviakov²⁴, L.N. Shtarkov²⁴, Y. Sirois²⁷,
 T. Sloan¹⁷, P. Smirnov²⁴, Y. Soloviev²⁴, D. South²¹, V. Spaskov⁸, A. Specka²⁷, H. Spitzer¹¹,

R. Stamen⁷, B. Stella³¹, J. Stiewe¹⁴, U. Straumann³⁷, M. Swart¹⁴, M. Taševský²⁹, S. Tchetchelnitski²³, G. Thompson¹⁹, P.D. Thompson³, N. Tobien¹⁰, F. Tomasz¹⁴, D. Traynor¹⁹, P. Truöl³⁷, G. Tsipolitis^{10,38}, I. Tsurin³⁵, J. Turnau⁶, J.E. Turney¹⁹, E. Tzamariudaki²⁵, S. Udluft²⁵, M. Urban³⁷, A. Usik²⁴, S. Valkár³⁰, A. Valkárová³⁰, C. Vallée²², P. Van Mechelen⁴, S. Vassiliev⁸, Y. Vazdik²⁴, A. Vichnevski⁸, M. Vorobiev²³, K. Wacker⁷, J. Wagner¹⁰, R. Wallny³⁷, B. Waugh²¹, G. Weber¹¹, M. Weber¹⁴, D. Wegener⁷, C. Werner¹³, M. Werner¹³, N. Werner³⁷, M. Wessels¹, G. White¹⁷, S. Wiesand³³, T. Wilksen¹⁰, M. Winde³⁵, G.-G. Winter¹⁰, Ch. Wissing⁷, M. Wobisch¹⁰, E.-E. Woehrling³, E. Wunsch¹⁰, A.C. Wyatt²¹, J. Žáček³⁰, J. Zálešák³⁰, Z. Zhang²⁶, A. Zhokin²³, F. Zomer²⁶, and M. zur Nedden¹⁰

¹ *I. Physikalisches Institut der RWTH, Aachen, Germany^a*

² *III. Physikalisches Institut der RWTH, Aachen, Germany^a*

³ *School of Physics and Space Research, University of Birmingham, Birmingham, UK^b*

⁴ *Inter-University Institute for High Energies ULB-VUB, Brussels; Universiteit Antwerpen (UIA), Antwerpen; Belgium^c*

⁵ *Rutherford Appleton Laboratory, Chilton, Didcot, UK^b*

⁶ *Institute for Nuclear Physics, Cracow, Poland^d*

⁷ *Institut für Physik, Universität Dortmund, Dortmund, Germany^a*

⁸ *Joint Institute for Nuclear Research, Dubna, Russia*

⁹ *CEA, DSM/DAPNIA, CE-Saclay, Gif-sur-Yvette, France*

¹⁰ *DESY, Hamburg, Germany*

¹¹ *Institut für Experimentalphysik, Universität Hamburg, Hamburg, Germany^a*

¹² *Max-Planck-Institut für Kernphysik, Heidelberg, Germany*

¹³ *Physikalisches Institut, Universität Heidelberg, Heidelberg, Germany^a*

¹⁴ *Kirchhoff-Institut für Physik, Universität Heidelberg, Heidelberg, Germany^a*

¹⁵ *Institut für experimentelle und Angewandte Physik, Universität Kiel, Kiel, Germany*

¹⁶ *Institute of Experimental Physics, Slovak Academy of Sciences, Košice, Slovak Republic^{e,f}*

¹⁷ *School of Physics and Chemistry, University of Lancaster, Lancaster, UK^b*

¹⁸ *Department of Physics, University of Liverpool, Liverpool, UK^b*

¹⁹ *Queen Mary and Westfield College, London, UK^b*

²⁰ *Physics Department, University of Lund, Lund, Sweden^g*

²¹ *Physics Department, University of Manchester, Manchester, UK^b*

²² *CPPM, CNRS/IN2P3 - Univ Mediterranee, Marseille - France*

²³ *Institute for Theoretical and Experimental Physics, Moscow, Russia^l*

²⁴ *Lebedev Physical Institute, Moscow, Russia^e*

²⁵ *Max-Planck-Institut für Physik, München, Germany*

²⁶ *LAL, Université de Paris-Sud, IN2P3-CNRS, Orsay, France*

²⁷ *LPNHE, Ecole Polytechnique, IN2P3-CNRS, Palaiseau, France*

²⁸ *LPNHE, Universités Paris VI and VII, IN2P3-CNRS, Paris, France*

²⁹ *Institute of Physics, Academy of Sciences of the Czech Republic, Praha, Czech Republic^{e,i}*

³⁰ *Faculty of Mathematics and Physics, Charles University, Praha, Czech Republic^{e,i}*

³¹ *Dipartimento di Fisica Università di Roma Tre and INFN Roma 3, Roma, Italy*

³² *Paul Scherrer Institut, Villigen, Switzerland*

³³ *Fachbereich Physik, Bergische Universität Gesamthochschule Wuppertal, Wuppertal, Germany*

³⁴ *Yerevan Physics Institute, Yerevan, Armenia*

³⁵ *DESY, Zeuthen, Germany*

³⁶ *Institut für Teilchenphysik, ETH, Zürich, Switzerland^j*

³⁷ *Physik-Institut der Universität Zürich, Zürich, Switzerland^j*

³⁸ *Also at Physics Department, National Technical University, Zografou Campus, GR-15773 Athens, Greece*

³⁹ *Also at Rechenzentrum, Bergische Universität Gesamthochschule Wuppertal, Germany*

⁴⁰ *Also at Institut für Experimentelle Kernphysik, Universität Karlsruhe, Karlsruhe, Germany*

⁴¹ *Also at Dept. Fis. Ap. CINVESTAV, Mérida, Yucatán, México^k*

⁴² *Also at University of P.J. Šafárik, Košice, Slovak Republic*

⁴³ *Also at CERN, Geneva, Switzerland*

⁴⁴ *Also at Dept. Fis. CINVESTAV, México City, México^k*

^a *Supported by the Bundesministerium für Bildung und Forschung, FRG, under contract numbers 05 H1 1GUA /1, 05 H1 1PAA /1, 05 H1 1PAB /9, 05 H1 1PEA /6, 05 H1 1VHA /7 and 05 H1 1VHB /5*

^b *Supported by the UK Particle Physics and Astronomy Research Council, and formerly by the UK Science and Engineering Research Council*

^c *Supported by FNRS-FWO-Vlaanderen, IISN-IKW and IWT*

^d *Partially Supported by the Polish State Committee for Scientific Research, grant no. 2P0310318 and SPUB/DESY/P03/DZ-1/99 and by the German Bundesministerium für Bildung und Forschung*

^e *Supported by the Deutsche Forschungsgemeinschaft*

^f *Supported by VEGA SR grant no. 2/1169/2001*

^g *Supported by the Swedish Natural Science Research Council*

ⁱ *Supported by the Ministry of Education of the Czech Republic under the projects INGO-LA116/2000 and LN00A006, by GAUK grant no 173/2000*

^j *Supported by the Swiss National Science Foundation*

^k *Supported by CONACyT*

^l *Partially Supported by Russian Foundation for Basic Research, grant no. 00-15-96584*

1 Introduction

Measurements of exclusive vector meson (VM) production in ep scattering at high energy:

$$e + p \rightarrow e + VM + Y, \quad (1)$$

have led to considerable recent progress towards an understanding of diffraction in terms of QCD [1–4]. The reaction is induced by a real or virtual photon and Y is either a proton (“elastic” scattering) or a baryonic system of mass M_Y which is much lower than the photon–proton centre of mass energy W (“proton dissociative” scattering). Particularly sensitive tests of QCD models are provided by the study of the helicity structure of the interaction and its t dependence, t being the square of the four-momentum transfer from the incident proton to the scattered system Y . The scope of this paper is to test diffractive dynamics through the extension of helicity amplitude extractions for exclusive ρ^0 electroproduction to larger values of $|t|$ than has previously been possible.

Three angles are defined to characterise the electroproduction of vector mesons decaying into two charged particles: Φ is the angle between the VM production plane (defined as the plane containing the virtual photon and the VM directions) and the electron scattering plane in the (γ^*p) centre of mass system, θ^* and φ are the polar and the azimuthal angles, respectively, of the positively charged decay particle in the VM rest frame, the quantisation axis being taken as the direction opposite to that of the outgoing Y system. In this paper, the distributions of the angles Φ and θ^* are analysed.

The angular distributions give access to spin density matrix elements, which are bilinear combinations of the helicity amplitudes $T_{\lambda_{VM}\lambda_\gamma}$, where λ_{VM} (λ_γ) is the vector meson (virtual photon) helicity [5]. In the case of vector meson electroproduction by unpolarised beams and their subsequent decay into two pseudoscalar particles ($\rho \rightarrow \pi^+\pi^-$, $\phi \rightarrow K^+K^-$), the Φ and θ^* distributions, integrated over the other two angles, are related to 5 of the 15 spin density matrix elements r_{ij}^k and r_{ij}^{kl} through the relations [5]

$$\frac{d\sigma}{d\Phi} \propto 1 + \sqrt{2\epsilon(1+\epsilon)} \cos \Phi (r_{00}^5 + 2r_{11}^5) - \epsilon \cos 2\Phi (r_{00}^1 + 2r_{11}^1) \quad (2)$$

$$\frac{d\sigma}{d\cos \theta^*} \propto 1 - r_{00}^{04} + (3 r_{00}^{04} - 1) \cos^2 \theta^*, \quad (3)$$

where ϵ is the polarisation parameter, i.e. the ratio of the longitudinal to transverse virtual photon fluxes. For this analysis $\epsilon \simeq 0.99$ [1].

Assuming natural parity exchange to hold ($T_{-\lambda_{VM}-\lambda_\gamma} = (-1)^{\lambda_{VM}-\lambda_\gamma} T_{\lambda_{VM}\lambda_\gamma}$), these five spin density matrix elements are related to the five independent complex helicity amplitudes by

the following relations:

$$\begin{aligned}
r_{00}^{04} &\propto \frac{1}{N} (|T_{00}|^2 + |T_{01}|^2) \\
r_{00}^5 &\propto \frac{1}{N} \operatorname{Re} (T_{00} T_{01}^\dagger) \\
r_{11}^5 &\propto \frac{1}{N} (\operatorname{Re} (T_{10} T_{11}^\dagger) - \operatorname{Re} (T_{10} T_{1-1}^\dagger)) \\
r_{00}^1 &\propto \frac{-1}{N} |T_{01}|^2 \\
r_{11}^1 &\propto \frac{1}{N} (T_{1-1} T_{11}^\dagger + T_{11} T_{1-1}^\dagger) \\
\text{with } N &= |T_{00}|^2 + |T_{11}|^2 + |T_{01}|^2 + 2 |T_{10}|^2 + |T_{1-1}|^2.
\end{aligned} \tag{4}$$

In the case of s -channel helicity conservation (SCHC), $\lambda_{VM} = \lambda_\gamma$, only the T_{00} and T_{11} helicity “non-flip” amplitudes are non-zero, $r_{00}^5 = r_{11}^5 = r_{00}^1 = r_{11}^1 = 0$ and the ratio R of the cross sections for longitudinal to transverse photons is given by $R = 1/\epsilon r_{00}^{04}/(1 - r_{00}^{04})$.

In recent years, the spin density matrix elements describing process (1) have been measured for the elastic electroproduction of ρ and ϕ mesons in the kinematic range $Q^2 > 2.5 \text{ GeV}^2$ and $|t| < 0.5 \text{ GeV}^2$ [1–3], Q^2 being the negative square of the virtual photon four-momentum. Three main features have emerged from these measurements:

- the dominance of the longitudinal T_{00} over the transverse T_{11} helicity non-flip amplitudes;
- the presence of a small but significant violation of SCHC, observed through the non-zero value of the r_{00}^5 matrix element, in which the dominant helicity single flip amplitude describes the transition from a transverse photon to a longitudinal vector meson (T_{01});
- values compatible with zero for the other amplitudes describing single (T_{10}) or double helicity flip (T_{1-1}).

These features are in agreement with calculations based on perturbative QCD (pQCD) [6–8]. In these approaches, vector meson electroproduction is described in the proton rest frame as the convolution of a virtual photon fluctuation into a $q\bar{q}$ pair at a long distance from the target, a hard interaction mediated by the exchange of two gluons (each of them must carry sufficiently large transverse momentum to resolve the $q\bar{q}$ pair and the proton structure), and the subsequent recombination of the quark pair into a vector meson. For massless quarks, the helicity of the $q\bar{q}$ pair is zero, such that the helicity of the virtual photon is transferred into the projection of the orbital angular momentum of the $q\bar{q}$ pair onto the γ^* direction. During the interaction, the helicity and the impact parameter of the quark pair are unchanged, but the orbital angular momentum can be modified through the transfer of the transverse momentum carried by the gluons. The helicity of the outgoing vector meson can thus be different from that of the incoming photon. Calculations show that such a helicity flip between the photon and the vector meson requires an asymmetric sharing of the photon longitudinal momentum by the quark and the antiquark [6–8].

For Q^2 above a few GeV^2 and $|t| \lesssim Q^2$, the following features are expected for the (predominantly imaginary) amplitudes:

- a ratio constant with t for the helicity conserving amplitudes $|T_{11}| / |T_{00}|$;
- a $\sqrt{|t|}$ dependence for the ratio of the single helicity flip to the non-flip amplitudes $|T_{01}| / |T_{00}|$ and $|T_{10}| / |T_{00}|$;
- a dependence linear with t for the ratio of the double flip to the non-flip amplitudes $|T_{1-1}| / |T_{00}|$;
- the hierarchy:

$$|T_{00}| > |T_{11}| > |T_{01}| > |T_{10}| > |T_{1-1}| . \quad (5)$$

These features are expected to hold for proton dissociative as well as for elastic scattering.

Compared to previous results [1–3], the present paper extends considerably the t range of the measurement of spin density matrix elements for ρ meson diffractive electroproduction

$$e + p \rightarrow e + \rho + Y ; \quad \rho \rightarrow \pi^+ \pi^- , \quad (6)$$

where the ρ mass range is defined by restricting the invariant mass $M_{\pi\pi}$ of the decay pions to the interval

$$0.6 < M_{\pi\pi} < 1.1 \text{ GeV} . \quad (7)$$

Elastic and proton dissociative data are combined, and the kinematic domain of the measurement is:

$$\begin{aligned} 2.5 < Q^2 < 60 \text{ GeV}^2 \\ 40 < W < 120 \text{ GeV} \\ 0 < t' < 3 \text{ GeV}^2 . \end{aligned} \quad (8)$$

The variable $t' = |t| - |t|_{min}$ is used for the analysis, where $|t|_{min}$ is the minimal value of $|t|$ kinematically required for the vector meson and the system Y to acquire their effective mass through longitudinal momentum transfer. The t' variable, which is very well approximated as the square of the transverse momentum of the scattered system Y , describes the transverse momentum transfer to the target and is thus the relevant dynamical variable. In the elastic case and for moderate Q^2 , $|t|_{min}$ is negligible and $t' \simeq |t|$.

The large t' domain covered by the present data allows for the first time a detailed study of the t' dependence of the helicity structure of diffractive vector meson electroproduction.

2 Experimental procedure

2.1 Event selection, kinematic variables and Monte Carlo simulations

The data used for the present analysis were taken with the H1 detector in 1997. The energies of the HERA proton and positron beams¹ were 820 GeV and 27.5 GeV, respectively. The

¹ In the following, the word electron will be used for both electrons and positrons.

integrated luminosity used for the analysis amounts to 6.0 pb^{-1} . The relevant parts of the detector, for which more details can be found in [1, 9], are the central tracking detector, the liquid argon (LAr) and the backward electromagnetic (SPACAL) calorimeters and the forward detectors, which are sensitive to energy flow close to the outgoing proton direction,² i.e. the proton remnant tagger (PRT) and the forward muon detector (FMD).

Events corresponding to reaction (6), in the kinematic range defined by relations (8), are selected by requesting the reconstruction of a cluster in the SPACAL calorimeter with energy larger than 17 GeV (the scattered electron candidate) and the reconstruction in the central tracking detector of the trajectories of exactly two charged particles (pion candidates) with opposite charges, transverse momenta larger than 0.1 GeV and polar angles confined within the interval $20^\circ < \theta < 160^\circ$. To reduce the background due to diffractive production of ϕ mesons, events with $M_{KK} < 1.04 \text{ GeV}$ are discarded, where M_{KK} is the invariant mass of the two hadron candidates when considered as kaons (no direct hadron identification is performed for this analysis). In order to reduce both QED radiative corrections and background contributions in which there are unreconstructed particles, a cut $E - p_z > 52 \text{ GeV}$ is applied. $E - p_z$ is the difference of the energies and the longitudinal momenta of the scattered electron (measured in the SPACAL) and the pion candidates (measured in the central tracking detector); it is expected to be close to twice the incident electron beam energy, i.e. 55 GeV, if no other particles have been produced except for the forward going system Y . To avoid backgrounds due to the diffractive production of systems decaying into two charged and additional neutral particles, all events are rejected in which a cluster, which is not associated with the electron or the two charged pion candidates, is reconstructed with polar angle larger than 20° and energy larger than 400 MeV (300 MeV) in the LAr (SPACAL) calorimeter.

The ρ three-momentum is computed as the sum of the two charged pion candidate momenta. The variable Q^2 is reconstructed using the double angle method [10]:

$$Q^2 = \frac{4E_0^2 \sin \theta_\rho (1 + \cos \theta_e)}{\sin \theta_e + \sin \theta_\rho - \sin(\theta_e + \theta_\rho)}, \quad (9)$$

where E_0 is the energy of the incoming electron and θ_e and θ_ρ are the scattered electron and ρ meson polar angles, respectively. The variable W is calculated using the Jacquet-Blondel method [11]:

$$W^2 = y \cdot s - \frac{p_{t,\rho}^2}{1 - y}, \quad \text{with } y = \frac{E_\rho - p_{z,\rho}}{2E_0}, \quad (10)$$

s being the square of the ep centre of mass energy and E_ρ , $p_{z,\rho}$ and $p_{t,\rho}$ being the energy, the longitudinal and the transverse momentum of the ρ meson, respectively. The electron transverse momentum is computed as

$$p_{t,e} = \frac{2E_0 - E_\rho + p_{z,\rho}}{\tan(\theta_e/2)}. \quad (11)$$

The variable t' is then determined from the scattered electron and ρ momentum components transverse to the beam direction as

$$t' \simeq (\vec{p}_{t,miss})^2 = (\vec{p}_{t,e} + \vec{p}_{t,\rho})^2. \quad (12)$$

² In the H1 convention, the z axis is defined by the colliding beams, the forward direction being that of the outgoing proton beam ($z > 0$) and the backward direction that of the electron beam ($z < 0$).

The selected events are classified in two categories, corresponding to the absence or presence of activity in the forward part of the H1 detector. An event is classified in the “notag” sample when no signal above noise is detected in the PRT and the FMD, and no track and no LAr cluster with energy larger than 400 MeV is reconstructed with polar angle $\theta < 20^\circ$. Conversely, events are classified in the “tag” sample if a signal is observed in either the PRT or the FMD, or if a track or a LAr cluster with energy larger than 400 MeV is reconstructed in the forward part of the H1 detector ($\theta < 20^\circ$).³ For the tagged events, a pseudorapidity interval of at least 2.2 units⁴ is required between the most backward track or LAr cluster with $\theta < 20^\circ$ (or the forward edge of the LAr calorimeter in the absence of track or cluster with $\theta < 20^\circ$), and the most forward charged pion candidate. To first approximation, the notag and tag samples could be attributed to the elastic and the proton dissociative processes, respectively. However, elastic events fall in the tag sample when $|t|$ is large enough for the scattered proton to hit the beam pipe walls or adjacent material, leading to secondary particles which give a signal in the forward detectors. This effect becomes significant for $t' \gtrsim 0.75 \text{ GeV}^2$. Conversely, proton dissociative events are classified in the notag sample for small masses, $M_Y \lesssim 1.6 \text{ GeV}$, or in the case of inefficiencies of the forward detectors.

The uncorrected $\pi^+\pi^-$ mass distributions are shown over the extended mass region $0.3 < M_{\pi\pi} < 1.3 \text{ GeV}$ in Fig. 1, separately for the tag and the notag samples, for $t' < 0.5 \text{ GeV}^2$ and for $0.5 < t' < 3 \text{ GeV}^2$. Clear ρ meson signals are visible in all distributions.

Monte Carlo simulations based on the DIFFVM program [12] including QED radiation [13] are used to describe the production and decay of ρ vector mesons in elastic and proton dissociative scattering, and to correct the data for acceptance, smearing and radiative effects. The simulations include the angular distributions corresponding to the measurements of the present analysis for the r_{00}^{04} matrix element ($\cos\theta^*$ distribution) and the $r_{00}^5 + 2r_{11}^5$ and $r_{00}^1 + 2r_{11}^1$ combinations (Φ distribution). Other angular distributions and correlations are taken in the SCHC approximation, and the $\cos\delta$ parameter, which describes the interference between the longitudinal and transverse amplitudes, is taken from the elastic scattering measurement [1] in the relevant Q^2 range. The exponential slope of the t distribution is $b_{el} = 7 \text{ GeV}^{-2}$ for elastic scattering [1] and $b_{pd} = 1.7 \text{ GeV}^{-2}$ for proton dissociative scattering, values which describe well the t' distribution of the present data. The t' -integrated cross section ratio for proton dissociative to elastic scattering is taken as 0.75 in the present Q^2 range [14]. For proton dissociative scattering, the M_Y spectrum is parameterised as $d\sigma/dM_Y^2 \propto 1/M_Y^2$.¹⁵ (see [15]) and corrections are applied for the loss of events with large M_Y values when particles of the dissociation system are reconstructed in the detector with polar angles $\theta > 20^\circ$. All these parameters have been varied in the simulation as a part of the systematic error analysis.

DIFFVM simulations have also been used for ω , ϕ and ρ' background studies (see next section). In all cases, the t slopes are chosen to be $b_{el} = 6 \text{ GeV}^{-2}$ for elastic scattering and $b_{pd} = 2.5 \text{ GeV}^{-2}$ for proton dissociative scattering. The ratios of the proton dissociative to elastic channels, integrated over t' , are 0.75. In the absence of measurements in electroproduction, the angular distributions for ω , ϕ (except for $\phi \rightarrow K^+K^-$ [3]) and ρ' are treated as isotropic.

³ In the case of proton dissociative scattering, this corresponds to an excitation mass of the target $M_Y \lesssim 25 \text{ GeV}$.

⁴ The pseudorapidity η of an object with polar angle θ is defined as $\eta = -\log \tan(\theta/2)$.

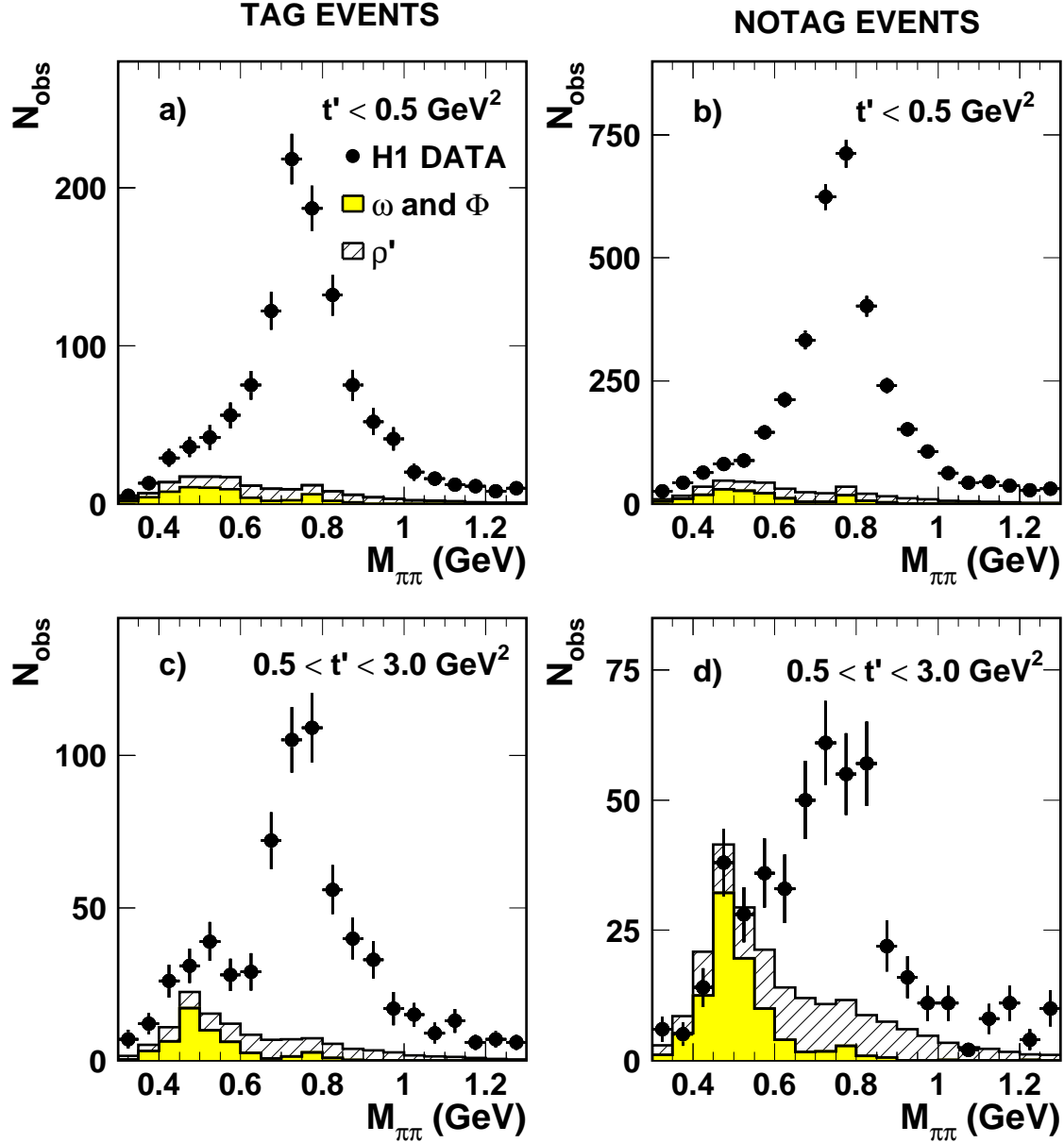


Figure 1: Uncorrected $\pi^+\pi^-$ mass distributions for the selected events with $0.3 < M_{\pi\pi} < 1.3 \text{ GeV}$. The shaded areas describe the ω and ϕ backgrounds and the hatched areas the ρ' background. a) and c) show tag events with $t' < 0.5 \text{ GeV}^2$ and $0.5 < t' < 3.0 \text{ GeV}^2$, respectively; b) and d) show notag events.

2.2 ω , ϕ and ρ' backgrounds

Diffractional electroproduction of ω and ϕ mesons can fake ρ production through the decay channels

$$\begin{aligned}\omega &\rightarrow \pi^+\pi^-\pi^0, \\ \phi &\rightarrow \pi^+\pi^-\pi^0, \quad \phi \rightarrow K_S^0 K_L^0,\end{aligned}\tag{13}$$

if the decay photons of the π^0 or the K_L^0 meson are not detected. This happens if the deposited energy is associated with the charged pion tracks or does not pass the detection threshold in the detector. The p_t imbalance of the event due to the loss of particles can then be interpreted as ρ production at large t' , following eq. (12). These background contributions, which are concentrated below the selected ρ mass range (7), are estimated using the Monte-Carlo simulations. The ratios of the production cross sections ω / ρ and ϕ / ρ are, for the present Q^2 range, taken as 0.09 [16] and 0.20 [3], respectively.

Another background reaction, particularly important for large t' in the selected mass range (7) is the electroproduction of ρ' mesons⁵ decaying into two charged pions and two π^0 :

$$\rho' \rightarrow \rho^+\pi^-\pi^0, \quad \rho^+ \rightarrow \pi^+\pi^0 \quad (+ c.c.).\tag{14}$$

Again, the non-detection of the two π^0 mesons induces p_t imbalance which fakes ρ production at large t' . No measurements exist in the relevant Q^2 range of the $\rho' \rightarrow \pi^+\pi^-\pi^0\pi^0$ to ρ cross section ratio. The ρ' contribution is thus determined in section 2.3 from the data themselves, using the events with $0.5 < t' < 3 \text{ GeV}^2$.

It is important to recognise that the presence of backgrounds at large t' values affects differently the tag and the notag samples defined in section 2.1. As mentioned there, genuine production of ρ mesons at large t' , either due to proton dissociative or elastic scattering, usually gives a signal in the forward detectors and contributes mainly to the tag sample. In contrast, ω , ϕ and ρ' background events, produced mainly at low t' but faking high t' ρ production, contribute to either the tag or the notag sample, depending on whether the proton dissociates and on the detector response. The ratio of the ρ signal to background at high t' is thus significantly higher in the tag sample than in the notag sample.

2.3 Determination of the ρ' background

In order to determine the ρ' background, a new variable, ζ , is introduced:

$$\zeta = \frac{\vec{p}_{t,miss} \cdot \vec{p}_{t,\rho}}{|\vec{p}_{t,miss}| |\vec{p}_{t,\rho}|}.\tag{15}$$

For ρ' events produced at low t' and faking high t' ρ production, $\vec{p}_{t,miss}$ is due to the two missing π^0 mesons and, in the present Q^2 range, is generally aligned along the (π^+, π^-) direction. This

⁵The detailed structure [17] of the states described in the past as the $\rho'(1600)$ meson is not relevant for the present study. The name ρ' is used to imply all vector meson states with mass in the range 1300-1700 MeV. In the simulations, the ρ' mass and width are taken as 1450 MeV and 300 MeV, respectively.

gives for the ρ' background a ζ distribution peaking around +1, as shown in Figs. 2a-b; the same effect is found for ω and ϕ production with the decay channels (13). In contrast, for genuine high t' ρ production, $\vec{p}_{t,miss}$ is the transverse momentum of the scattered proton or baryonic system, leading to a flatter ζ distribution, with maxima at -1 and $+1$. The ζ and the Φ distributions are strongly correlated: positive ζ values correspond to Φ angles close to 0° and 360° , whereas for negative ζ , central Φ values are selected. This is visible in Figs. 2c-d, which compare background events (for which ζ is mostly positive) to ρ events (for which negative ζ values dominate).

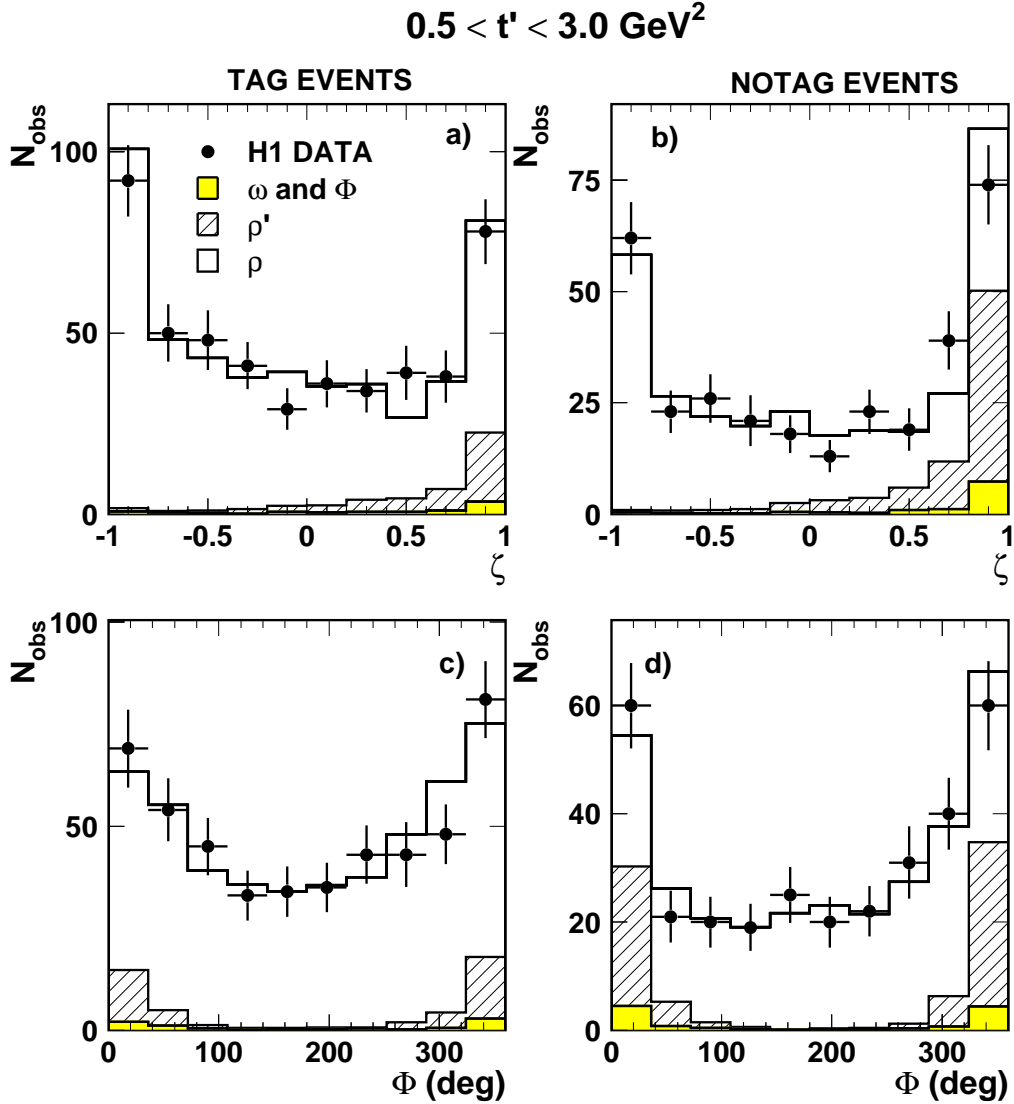


Figure 2: Distributions of a-b) the ζ and c-d) the Φ variables of the selected events in the mass range (7) with $0.5 < t' < 3 \text{ GeV}^2$, in the tag (a and c) and in the notag (b and d) sample. The shaded areas describe the ω and ϕ background as obtained from the simulations. The hatched areas correspond to the ρ' background and the open areas to the ρ contribution, as determined using the iterative fitting procedure described in section 2.3.

An iterative fitting procedure is performed to estimate the ρ' background, whilst dealing

with this $\zeta - \Phi$ correlation. After subtraction of the ω and ϕ backgrounds using the Monte Carlo simulations, the selected events in the mass range (7) are divided into four subsamples: tag events and notag events, separately with $\zeta < 0$ and with $\zeta > 0$. Each of these four samples contains two contributions, due to genuine ρ production and to ρ' background. These eight contributions (eight unknowns) are determined through an overconstrained fit, performed using the MINUIT package [18], to the numbers of events in the four samples (four measurements), under the following six constraints, obtained using the Monte Carlo simulations:

- i. two constraints describe the asymmetry of the ζ distribution of ρ events (i.e. the ratio of the numbers of events with $\zeta < 0$ and with $\zeta > 0$), separately for the tag and for the notag sample (see the open areas in Figs. 2a and b, respectively);
- ii. similarly, two constraints describe the asymmetry of the ζ distribution for ρ' events, separately for the tag and notag samples (hatched areas);
- iii. the last two constraints, defined separately for $\zeta < 0$ and for $\zeta > 0$, are the probabilities for any ρ' event (elastic or proton dissociative) to be tagged; the ratio of the proton dissociative to elastic ρ' production cross sections is taken as 0.75 in the simulation.

An estimate of the ρ' background is thus obtained, and its Φ distribution is computed using the simulation. Relation (2) is then fitted to the Φ distribution in the tag sample, fully corrected for background, acceptance, smearing and radiative effects, to extract values of the spin density matrix element combinations $r_{00}^5 + 2r_{11}^5$ and $r_{00}^1 + 2r_{11}^1$. These values are fed back into the ρ simulation, leading to a modification of the simulated Φ and hence ζ distributions, which provides new values for the constraints describing the asymmetry of the latter (see item i. above). The fitting procedure is repeated, and the iterative process converges after a few steps to stable background estimates, independent of the starting values of the spin density matrix elements in the ρ Monte Carlo simulation.

Fig. 2 presents the ζ and Φ distributions of the selected events with $0.5 < t' < 3 \text{ GeV}^2$, separately for the tag and the notag samples. They are well described by the superposition of the ω and ϕ background, the ρ' background and the ρ contribution, as determined from the iterative fitting procedure. The dominant background is found to be from ρ' production and, as expected, the backgrounds are larger in the notag sample and affect mainly the $\zeta > 0$ region.

This procedure thus provides an estimate of the ρ'/ρ cross section ratio for $0.5 < t' < 3 \text{ GeV}^2$. This estimate is extended to $t' < 0.5 \text{ GeV}^2$, under the assumptions quoted in section 2.1 for the t slopes and for the proton dissociative to elastic cross section ratio.

The background contributions are shown in Figs. 1a-d. After background subtraction, relativistic Breit-Wigner functions, with the Ross-Stodolsky skewing parameter [19] left free, are fitted to the fully corrected data, yielding ρ mass and width values in excellent agreement with expectations [17] and good χ^2 values. The data are thus very well described by diffractive ρ production with contributions of additional ω , ϕ and ρ' backgrounds. The elastic cross section at low t agrees with previous measurements [1].

2.4 Systematic errors

In addition to the effect of varying the number of bins, the systematic uncertainties affecting the measurements described in section 3 are grouped into three classes:

- **Uncertainties in the amount and shape of the backgrounds**

The amount of ω and ϕ backgrounds is varied by $\pm 50\%$. The uncertainty in the amount of ρ' background for $t' > 0.5 \text{ GeV}^2$ is estimated by varying, for the fit procedure, the ζ separation between the samples (at $-0.4, -0.2, 0.2$ and 0.4 instead of 0). The fractions of background events with $\zeta < 0$ (see Figs. 2a-b) are also multiplied by 2 and 0.5. For $t' < 0.5 \text{ GeV}^2$, the ρ'/ρ cross section ratio is changed by $\pm 50\%$. The shape of the background in the Φ distribution (section 3.1) is modified by keeping the total amount fixed, but changing the fraction assigned to the two extreme Φ bins by $\pm 50\%$ (see Figs. 2c-d). For the $\cos\theta^*$ distribution (section 3.2), the shape of the background is varied from flat to the same distribution as that of the ρ signal. The following model uncertainties in the background simulations are also included: the t slopes are varied ($b_{el} = 6 \pm 1 \text{ GeV}^{-2}$ and $b_{pd} = 2.5 \pm 1 \text{ GeV}^{-2}$), the proton dissociative to elastic production cross section ratio is changed from 0.75 to 0.5 and to 1.0, and the mass and width of the ρ' meson are varied: $M_{\rho'} = 1450 \pm 150 \text{ MeV}$ and $\Gamma_{\rho'} = 300 \pm 150 \text{ MeV}$.

- **Uncertainties affecting ρ production**

For the simulation of ρ meson production, the t slopes ($b_{el} = 7 \pm 1 \text{ GeV}^{-2}$ and $b_{pd} = 1.7_{-0.7}^{+0.8} \text{ GeV}^{-2}$) and the proton dissociative to elastic production cross section ratio (0.75 ± 0.25) are changed, and the cross section dependences on Q^2 and W are varied within limits of the measurements in [1]. Furthermore, the M_Y^2 spectrum as implemented in DIFFVM is varied from $1/M_Y^{2.15}$ to $1/M_Y^{1.85}$ and to $1/M_Y^{2.45}$.

- **Uncertainties in the detector response**

The energy threshold for the detection of LAr clusters not associated to tracks is varied between 300 MeV and 500 MeV; the efficiencies of the PRT and FMD are modified within experimental errors; the measurement of the polar angle of the scattered electron is changed by $\pm 0.5 \text{ mrad}$ and the uncertainties in the trigger and the tracker efficiencies are included.

For the measurements in section 3, the dominant systematic error is due to the uncertainty in the shapes of the backgrounds.

3 t' dependences of spin density matrix elements

3.1 Φ distributions and determination of $(r_{00}^5 + 2r_{11}^5)$ and $(r_{00}^1 + 2r_{11}^1)$

Measurements of the spin density matrix element combinations $r_{00}^5 + 2r_{11}^5$ and $r_{00}^1 + 2r_{11}^1$ are obtained from fits of eq. (2) to the Φ distributions, fully corrected for the presence of backgrounds and for acceptance, smearing and QED radiative effects, in the five t' bins shown in

Fig. 3a. For $0.5 < t' < 3.0 \text{ GeV}^2$, only the tag sample is used, in view of the much larger background in the notag sample (compare Figs. 1c-d). Given the small backgrounds (Figs. 1a-b) and in order to improve the statistical precision of the measurement, the tag and the notag samples are merged for $t' < 0.5 \text{ GeV}^2$. The measurements are given in Table 1 and presented in Figs. 4a and 4b, together with previous measurements for $t' < 0.5 \text{ GeV}^2$ in similar W and Q^2 ranges ($Q^2 > 2.5 \text{ GeV}^2$ from ref. [1] and $Q^2 > 3.0 \text{ GeV}^2$ from ref. [2]).

Element	t' (GeV^2)	$\langle t' \rangle$ (GeV^2)	Measurement		
$r_{00}^5 + 2r_{11}^5$	$t' < 0.08$	0.037	0.064	± 0.012	± 0.040
	$0.08 < t' < 0.2$	0.132	0.087	± 0.014	± 0.017
	$0.2 < t' < 0.5$	0.320	0.201	± 0.014	± 0.037
	$0.5 < t' < 1.0$	0.700	0.198	± 0.017	± 0.032
	$1.0 < t' < 3.0$	1.620	0.290	± 0.023	± 0.049
$r_{00}^1 + 2r_{11}^1$	$t' < 0.08$	0.037	-0.006	± 0.025	± 0.020
	$0.08 < t' < 0.2$	0.132	-0.022	± 0.027	± 0.034
	$0.2 < t' < 0.5$	0.320	-0.119	± 0.028	± 0.052
	$0.5 < t' < 1.0$	0.700	-0.134	± 0.034	± 0.066
	$1.0 < t' < 3.0$	1.620	-0.176	± 0.046	± 0.076
r_{00}^{04}	$t' < 0.08$	0.037	0.678	± 0.013	± 0.015
	$0.08 < t' < 0.2$	0.132	0.683	± 0.014	± 0.014
	$0.2 < t' < 0.5$	0.320	0.662	± 0.015	± 0.025
	$0.5 < t' < 1.0$	0.700	0.665	± 0.019	± 0.026
	$1.0 < t' < 3.0$	1.620	0.708	± 0.023	± 0.035

Table 1: Measurement of the spin density matrix element combinations $r_{00}^5 + 2r_{11}^5$, $r_{00}^1 + 2r_{11}^1$ and r_{00}^{04} in five bins of t' . The first errors are statistical, the second systematic.

Significant helicity non-conservation is observed in Fig. 4a for the combination $r_{00}^5 + 2r_{11}^5$ (SCHC would imply a zero value of the combination). The r_{00}^5 matrix element is proportional (see relations (4)) to the product of the dominant non-flip amplitude T_{00} and the T_{01} amplitude, expected to be the largest helicity flip amplitude (see relations (5)). In contrast, the r_{11}^5 matrix element has a contribution from the product of the non-dominant non-flip amplitude T_{11} and the non-dominant single flip amplitude T_{10} , and a contribution dependent on the double flip amplitude. The strong t' dependence of the $r_{00}^5 + 2r_{11}^5$ combination is thus attributed mainly to the predicted [6–8] $\sqrt{t'}$ dependence of the ratio of the T_{01} to the non-flip amplitudes. Note that the t' dependence of the $r_{00}^5 + 2r_{11}^5$ combination is not exactly $\propto \sqrt{t'}$, as expected for the single-flip to the non-flip amplitude ratio, since it also involves the effect of the single and double-flip amplitudes in the denominator N of relations (4).

The values for $r_{00}^1 + 2r_{11}^1$ are shown in Fig. 4b. They are significantly different from zero and negative, which implies violation of SCHC. This is the first observation of a significant non-zero value of the $r_{00}^1 + 2r_{11}^1$ spin density matrix element combination. The r_{00}^1 element, which gives a negative contribution (see relations (4)), is proportional to the square of the single flip amplitude T_{01} . The r_{11}^1 element is proportional to the product of the non-dominant non-flip amplitude T_{11} and the double flip amplitude. The sign of the combination thus gives information on the relative strength of the $T_{01}T_{01}^\dagger$ and $T_{11}T_{1-1}^\dagger$ products of amplitudes. It confirms that the

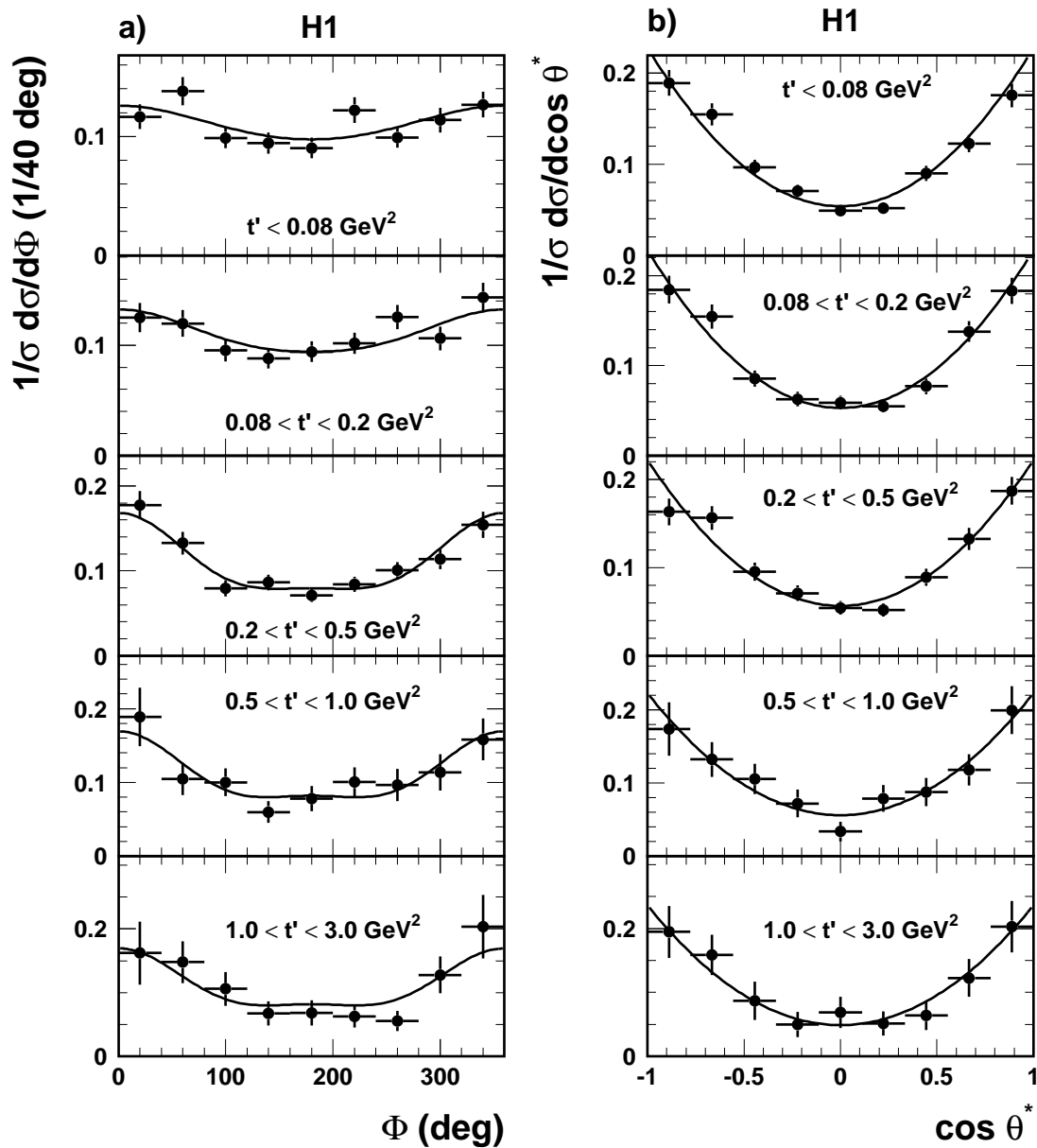


Figure 3: Normalised cross sections for ρ electroproduction in five bins in t' . The superimposed curves show the results of fits of a) relation (2) and b) relation (3). The error bars represent the statistical errors.

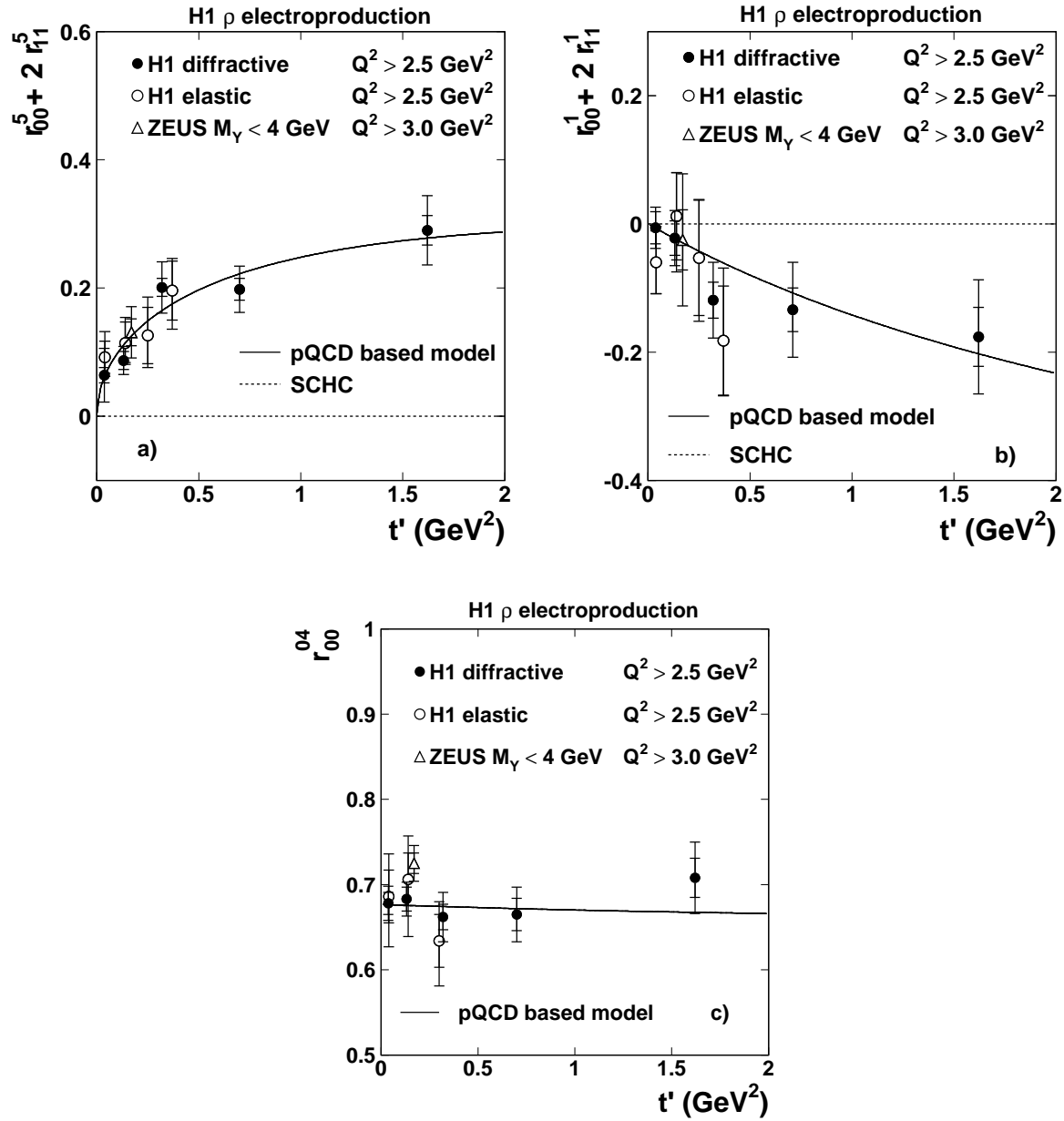


Figure 4: Measurement of a) $r_{00}^5 + 2r_{11}^5$, b) $r_{00}^1 + 2r_{11}^1$, c) r_{00}^{04} as a function of t' , for the present analysis and for refs. [1] (labeled “H1 elastic”) and [2] (labeled “ZEUS $M_Y < 4 \text{ GeV}$ ”). The inner error bars represent the statistical errors, the full error bars include the systematic errors added in quadrature. The full curves correspond to the predictions of the model [8] with parameters extracted from the fit described in section 4. The dashed lines in a) and b) correspond to SCHC.

T_{01} amplitude is significantly larger than the double flip amplitude in the present kinematical domain. The t' dependence of the $r_{00}^1 + 2r_{11}^1$ combination is expected to be linear, up to effects of the single and double-flip amplitudes in the denominator N of relations (4).

3.2 $\cos \theta^*$ distributions and determination of r_{00}^{04}

The r_{00}^{04} spin density matrix element is extracted from the $\cos \theta^*$ distribution using relation (3). Fig. 3b presents the fully corrected $\cos \theta^*$ distributions for five bins in t' . The normalisations of the ω , ϕ and ρ' backgrounds are estimated as described above. The shape of the background is determined from the data and found to be flat. This is done by comparing the $\cos \theta^*$ distributions for the events with $\zeta < 0$ and $\zeta > 0$, which differ in the data whereas they are predicted to be similar by the ρ Monte Carlo simulation. The difference is attributed to background.

The extracted values of r_{00}^{04} are presented in Table 1 and in Fig. 4c, together with previous measurements at low t' values in the same Q^2 and W range. No significant variation of r_{00}^{04} with t' is observed. This is expected from relation (4) in view of the predicted t' independence of the ratio $|T_{11}|/|T_{00}|$, with small corrections from the other amplitudes. This observation implies that the slopes of the exponentially falling t distributions for the transverse and longitudinal s -channel helicity conserving amplitudes, T_{00} and T_{11} , are very similar.

4 QCD description of the measurements

Perturbative QCD calculations for vector meson electroproduction assume the factorisation of the non-perturbative from the perturbative contributions to the amplitudes. Collinear factorisation has been demonstrated for longitudinal photons [20], but logarithmic singularities are manifest for the transverse photon polarisation when the fraction z of the longitudinal momentum carried by the quark approaches 0 or 1. Non-perturbative effects were suggested to damp these singularities [21], in which case perturbative calculations become problematic. However, as noted in [22], these contributions cannot be large,⁶ and in the models [6–8] pQCD is expected to be valid also for the transverse amplitudes.

In the models [6–8] all amplitudes are proportional, in the leading $\log(Q^2)$ approximation, to the gluon density in the proton (except for non-perturbative contributions in the double-flip amplitude).⁷ More specifically, in the model of Ivanov and Kirschner [8], the gluon distribution in the proton $xG(x, \tilde{Q}^2)$ is probed at the hard scale $\tilde{Q}^2 = z(1-z)Q^2 \leq Q^2/4$. Following a suggestion of Martin, Ryskin and Teubner [22], the scale dependence of the gluon density in the leading $\log \tilde{Q}^2$ approximation is parameterised as $G(x, \tilde{Q}^2) = G(x, Q_0^2) [\tilde{Q}^2/Q_0^2]^\gamma$, where the gluon anomalous dimension γ is taken as Q^2 independent. This permits the singularities as $z \rightarrow 0, 1$ to be avoided and factorisation is effectively (but not necessarily exactly) restored for the transverse amplitudes.

⁶Large non-perturbative contributions to the transverse amplitudes would imply a t slope similar to the non-perturbative photoproduction case, $b_T \simeq 10 \text{ GeV}^{-2}$, significantly larger than for the longitudinal cross section ($b_L \simeq 6 \text{ GeV}^{-2}$). This is inconsistent with the very weak t dependence of the r_{00}^{04} matrix element (section 3.2).

⁷For large mass vector mesons and/or large Q^2 , skewed parton distributions should be used.

The absolute values and the Q^2 and t dependences of the four independent ratios⁸ of the amplitudes $T_{\lambda_{VM}\lambda_\gamma}$ are predicted by the model [8] with two independent parameters: the effective gluon anomalous dimension γ , and the effective mass m of the incoming $q\bar{q}$ pair. These two free parameters are obtained from a fit to the t' dependence of the 15 measurements of spin density matrix elements in the present analysis.⁹ The fit gives an excellent description of the data: $\chi^2/ndf = 0.41$ when the full errors are used and $\chi^2/ndf = 1.71$ for statistical errors only. The fitted values of the parameters are $\gamma = 0.60 \pm 0.09$ and $m = 0.58 \pm 0.04$ GeV. The errors are the quadratic combination of the statistical and systematic errors, the latter obtained by repeating the fits with the data shifted by each systematic uncertainty in turn. The dominant error comes from the uncertainty in the background shape. The results of the fit are shown as solid lines in Figs. 4a-c. As can be observed, the 11 low t' measurements of ref. [1], which correspond to the same Q^2 and W ranges as the present data, are also very well described; their inclusion in the fit does not change the quantitative results significantly.

According to the parton distributions in PDFLIB [23], the extracted value of γ corresponds to the Q^2 evolution of the gluon density for $\tilde{Q}^2 \simeq 5.0$ GeV² which is much higher than the average $\langle \tilde{Q}^2 \rangle \leq \langle Q^2/4 \rangle \simeq 1.3$ GeV² in the data. The γ parameter was introduced in the model to restore factorisation which is otherwise broken by end-point effects ($z \rightarrow 0, 1$) in the transverse amplitudes. It does not need to be strictly interpreted as describing the evolution of the gluon distribution in the proton at the specified \tilde{Q}^2 [24]. On the other hand, the disagreement may suggest that the model does not apply in the full Q^2 range of the present data. The parameter $m = 0.58 \pm 0.04$ GeV is slightly below the ρ meson mass but belongs to a mass range where the quark pair is highly likely to recombine into a ρ meson (cf the parton-hadron duality arguments in [22]).

5 Conclusions

A measurement has been performed of ρ meson diffractive electroproduction in the range $2.5 < Q^2 < 60$ GeV², $40 < W < 120$ GeV and $0 < t' < 3$ GeV². The r_{00}^{04} spin density matrix element and the combinations $r_{00}^5 + 2r_{11}^5$ and $r_{00}^1 + 2r_{11}^1$ have been measured as functions of t' .

No significant t' dependence is observed for r_{00}^{04} . A significant violation of s -channel helicity conservation, increasing with t' , is observed in the $r_{00}^5 + 2r_{11}^5$ combination. It is consistent with a $\sqrt{t'}$ dependence of the ratio of the amplitude T_{01} to the non-flip amplitudes, T_{01} being the amplitude for the transition from a transverse photon to a longitudinal ρ meson. The $r_{00}^1 + 2r_{11}^1$ combination is different from zero and negative; this is the first observation of a significant non-zero value of this combination. The sign gives information on the relative strength of the $T_{01}T_{01}^\dagger$ and $T_{11}T_{1-1}^\dagger$ amplitude products. Together with the $r_{00}^5 + 2r_{11}^5$ measurement, it confirms that the T_{01} amplitude is relatively large in the present kinematical domain, and significantly larger than the double flip amplitude.

A fit of the pQCD model of Ivanov and Kirschner [8] to the present 15 measurements of spin density matrix elements gives a good description of the t' dependence of the data. The

⁸Under the assumptions of natural parity exchange and of purely imaginary amplitudes.

⁹The amplitude T_{1-1} , which contains a non-perturbative part in [8] and is expected to be very small (see relations (5)), can be set to zero or included as a free parameter in the fit without affecting the results.

value $\gamma = 0.60 \pm 0.09$ is obtained for the effective parameter describing the Q^2 dependence of the gluon density and $m = 0.58 \pm 0.04$ GeV is extracted for the average effective mass of the incoming $q\bar{q}$ pair. Thus the data are broadly compatible with a diffractive mechanism based on the exchange of two gluons, with non-conservation of s -channel helicity occurring only when the photon longitudinal momentum is shared asymmetrically between the quark and the antiquark [6–8].

Acknowledgements

We are grateful to the HERA machine group whose outstanding efforts have made and continue to make this experiment possible. We thank the engineers and technicians for their work in constructing and now maintaining the H1 detector, our funding agencies for financial support, the DESY technical staff for continual assistance, and the DESY directorate for the hospitality which they extend to the non DESY members of the collaboration. We also thank M. Diehl, D.Yu. Ivanov, I.P. Ivanov and R. Kirschner for helpful contributions.

References

- [1] C. Adloff *et al.* [H1 Collaboration], Eur. Phys. J. **C13** (2000) 371 [hep-ex/9902019].
- [2] J. Breitweg *et al.* [ZEUS Collaboration], Eur. Phys. J. **C12** (2000) 393 [hep-ex/9908026];
J. Breitweg *et al.* [ZEUS Collaboration], Eur. Phys. J. **C6** (1999) 603 [hep-ex/9808020].
- [3] C. Adloff *et al.* [H1 Collaboration], Phys. Lett. **B483** (2000) 360 [hep-ex/0005010].
- [4] S. Chekanov *et al.* [ZEUS Collaboration], DESY-02-008, submitted to Eur. Phys. J. **C** [hep-ex/0201043];
C. Adloff *et al.* [H1 Collaboration], Phys. Lett. **B483** (2000) 23 [hep-ex/0003020];
C. Adloff *et al.* [H1 Collaboration], Eur. Phys. J. **C10** (1999) 373 [hep-ex/9903008].
- [5] K. Schilling and G. Wolf, Nucl. Phys. **B61** (1973) 381.
- [6] I. Royen and J. Cudell, Nucl. Phys. **B545** (1999) 505 [hep-ph/9807294]; I. Royen, Phys. Lett. **B513** (2001) 337 [hep-ph/0006044].
- [7] E. Kuraev, N. Nikolaev and B. Zakharov, JETP Lett. **68** (1998) 696 [hep-ph/9809539].
- [8] D.Yu. Ivanov and R. Kirschner, Phys. Rev. **D58** (1998) 114026 [hep-ph/9807324].
- [9] I. Abt *et al.* [H1 Collaboration], Nucl. Instr. Meth. **A386** (1997) 310 and 348;
R. D. Appuhn *et al.* [H1 SPACAL Group Collaboration], Nucl. Instr. Meth. **A386** (1997) 397.
- [10] S. Bentvelsen, J. Engelen and P. Kooijman, in Proc. of the Workshop on Physics at HERA, W. Buchmüller and G. Ingelman ed., Hamburg (1992) 23; K.C. Hoeger, *ibid*, p 43.

- [11] F. Jacquet, A. Blondel, DESY 79-048 (1979) 377.
- [12] B. List and A. Mastroberardino, in Proc. of the Workshop on Monte Carlo Generators for HERA Physics, A.T. Doyle et al. ed., DESY-PROC-1999-02 (1999) 396.
- [13] A. Kwiatkowski, H.-J. Möhring and H. Spiesberger, Comput. Phys. Commun. 69 (1992), 155 and Proc. of the Workshop on Physics at HERA, W. Buchmüller and G. Ingelman ed., Hamburg (1992) 1294.
- [14] C. Adloff *et al.* [H1 Collaboration], Z. Phys. **C75** (1997) 607 [hep-ex/9705014].
- [15] K. Goulianos, Phys. Rep. **101** (1983) 169.
- [16] J. Breitweg *et al.* [ZEUS Collaboration], Phys. Lett. **B487** (2000) 273 [hep-ex/0006013].
- [17] Particle Data Group, D. Groom *et al.*, Eur. Phys. J. **C15** (2000) 1.
- [18] MINUIT, Cern Program Library Long Writeup D506.
- [19] M. Ross and L. Stodolsky, Phys. Rev. **149** (1966) 1173.
- [20] J. Collins, L. Frankfurt and M. Strikman, Phys. Rev. **56** (1997) 2982 [hep-ph/9611433]; E. Levin *et al.*, Z. Phys. **C74** (1997) 671, and ref. therein [hep-ph/9606443].
- [21] S. Brodsky *et al.*, Phys. Rev. **50** (1994) 3134 [hep-ph/9402283].
- [22] A. Martin, M. Ryskin and T. Teubner, Phys. Rev. **D55** (1997) 4329 [hep-ph/9609448].
- [23] H. Plochow-Besch, W5051 PDFLIB, User's Manual, version 8.04.
- [24] R. Kirschner, private communication.